

Submolecular Imaging by Noncontact Atomic Force Microscopy with an Oxygen Atom Rigidly Connected to a Metallic Probe

Harry Mönig,^{*,†,‡} Diego R. Hermoso,^{§,||} Oscar Díaz Arado,^{†,‡,||} Milica Todorović,[§] Alexander Timmer,^{†,‡} Simon Schüter,^{†,‡} Gernot Langewisch,^{§,⊥} Rubén Pérez,^{†,‡} and Harald Fuchs^{†,‡}

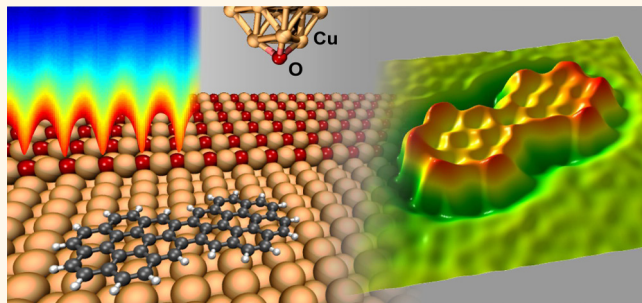
[†]Physikalisches Institut, Westfälische Wilhelms-Universität Münster, Wilhelm-Klemm-Strasse 10, 48149 Münster, Germany

[‡]Center for Nanotechnology (CeNTech), Heisenbergstrasse 11, 48149 Münster, Germany

[§]Departamento de Física Teórica de la Materia Condensada and [⊥]Condensed Matter Physics Center (IFIMAC), Universidad Autónoma de Madrid, 28049 Madrid, Spain

Supporting Information

ABSTRACT: In scanning probe microscopy, the imaging characteristics in the various interaction channels crucially depend on the chemical termination of the probe tip. Here we analyze the contrast signatures of an oxygen-terminated copper tip with a tetrahedral configuration of the covalently bound terminal O atom. Supported by first-principles calculations we show how this tip termination can be identified by contrast analysis in noncontact atomic force and scanning tunneling microscopy (NC-AFM, STM) on a partially oxidized Cu(110) surface. After controlled tip functionalization by soft indentations of only a few angstroms in an oxide nanodomain, we demonstrate that this tip allows imaging an organic molecule adsorbed on Cu(110) by constant-height NC-AFM in the repulsive force regime, revealing its internal bond structure. In established tip functionalization approaches where, for example, CO or Xe is deliberately picked up from a surface, these probe particles are only weakly bound to the metallic tip, leading to lateral deflections during scanning. Therefore, the contrast mechanism is subject to image distortions, artifacts, and related controversies. In contrast, our simulations for the O-terminated Cu tip show that lateral deflections of the terminating O atom are negligible. This allows a detailed discussion of the fundamental imaging mechanisms in high-resolution NC-AFM experiments. With its structural rigidity, its chemically passivated state, and a high electron density at the apex, we identify the main characteristics of the O-terminated Cu tip, making it a highly attractive complementary probe for the characterization of organic nanostructures on surfaces.



KEYWORDS: noncontact atomic force microscopy, tip functionalization, copper oxide, high-resolution imaging, organic molecules, contrast mechanism

The methodology in noncontact atomic force microscopy (NC-AFM) has seen impressive developments in recent years. While atomic resolution was achieved early on various substrates,¹ it was only in 2009 when the first submolecular resolution of an organic molecule was demonstrated, resolving its internal bond structure.² This milestone was achieved by using a CO-functionalized tip in conjunction with a tuning fork based force sensor in the qPlus configuration operated at low temperatures (5 K) and with oscillation amplitudes below one angstrom. It triggered a number of studies with outstanding results, including the visualization of the charge distribution,^{3–6} bond order discrimination,⁷ characterization of complex structures,^{8,9} self-assembly,^{10–13} and chemical on-surface reactions of organic molecules.^{14,15}

In most of these experiments, the probe tip was functionalized by picking up a single CO molecule from the surface, which reduces the chemical reactivity of the tip apex. This lowers the probability that the investigated molecule is displaced or picked up from the surface when imaging at small tip–sample distances, where repulsive forces become dominant. This way of tip functionalization can be done in a very controlled fashion,^{16,17} but the contrast formation mechanisms with CO-functionalized tips in constant-height

Received: October 16, 2015

Accepted: November 25, 2015

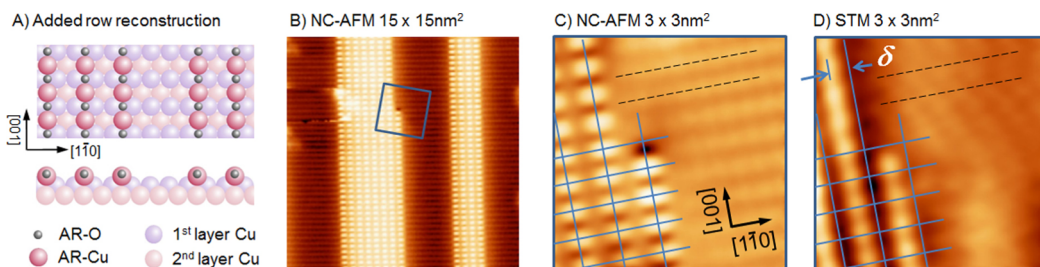


Figure 1. (A) Top and side view of a structural model of the striped Cu(110)-(2 × 1)O added-row reconstruction. (B) Overview NC-AFM image with two Cu oxide domains (bright stripes) separated by pure Cu(110) domains (darker areas). (C) Zoomed-in NC-AFM image as indicated by the blue square in B. (D) STM image recorded on the same area as in C without oscillating the tip. Lateral drift between the recording of the images in C and D was determined to be negligible (Figure S1). Therefore, the atomic sites as marked by the blue grid lines can be directly compared. Imaging parameters NC-AFM: $\Delta f = -6.0$ Hz; bias voltage $U_{\text{gap}} = 0.0$ V (B and C); STM: current set-point $I = 0.5$ nA; $U_{\text{gap}} = 0.1$ V (D).

NC-AFM imaging are nontrivial, involving site-dependent deflection of the CO molecule during scanning.^{7,18,19} As a result of this lateral flexibility of the probe, image distortions in conjunction with an apparent sharpening of the contrast and a related bond elongation have been observed.^{7,20} Related to these artifacts, there is currently an ongoing debate about fictitious bonds in image contrasts of molecular assemblies.^{11,21,22} There have been efforts to functionalize NC-AFM tips with other molecules or atoms picked up from the surface. In particular, tip functionalization with small organic molecules or single atoms such as Cl, Br, and Xe was successfully applied to enhance the resolution.^{2,13,23} But even for single atoms adsorbed at the tip apex, the imaging mechanism involves a considerable lateral displacement of the probe particle during scanning.^{21,22} It is important to note here that in all the mentioned studies the probe particle is not covalently connected to the tip. As a result, it is subject to lateral displacements and the related artifacts. Therefore, in the pool of currently established approaches for tip functionalization, a chemically passivated and rigid tip is highly desired.

In the present study, we show that the structural and chemical stability of an O-terminated Cu tip allows to image dicoronylene (DCLN), an organic molecule adsorbed on the Cu(110) surface with submolecular resolution. The experiment was performed on a partially oxidized (2 × 1)-O reconstructed Cu(110) surface, which typically features striped oxide domains extending along the [001] direction.²⁴ We achieve tip functionalization by slight indentations of the tip in one of the copper oxide domains and, subsequently, recording image data as tip fingerprints. To be able to unambiguously verify the O-termination of the tip in such an experiment, we performed an in-depth contrast analysis on this oxidized surface, employing three-dimensional (3D) NC-AFM and scanning tunneling microscopy (STM) experiments in conjunction with density-functional theory (DFT) and nonequilibrium Greens function (NEGF) calculations. By simulations of site-dependent force–distance curves, we demonstrate that the O-terminated Cu tip exhibits a significantly weaker interaction with the surface as compared to a pure Cu tip, showing that the oxygen termination chemically passivates the tip apex. In addition, the simulations indicate that the O-terminated tip remains structurally stable, whereas the Cu tip exhibits pronounced atomic relaxations upon approach. The low chemical reactivity and structural stability of the O-terminated Cu tip are important factors for the successful high-resolution NC-AFM experiment conducted on the DCLN molecule. The high structural stability of this tip is supported by simulated line

scans across a C–C bond of the DCLN, revealing that lateral displacements of the oxygen atom at the tip apex during scanning in the repulsive force regime are negligible. A comparison of experimentally and theoretically determined bond lengths discloses a considerable uncertainty of about 16%, but no systematic overestimation of bond lengths as observed in experiments with CO-functionalized tips.⁷ The imaging mechanism of this tip is investigated by a comparison of experimental and simulated force–distance curves. Being able to exclude tip flexibility as a major factor in the imaging process allows a detailed discussion about the contrast formation in high-resolution NC-AFM experiments in the repulsive regime.

RESULTS AND DISCUSSION

Figure 1A displays a structural model of the striped oxygen-induced reconstruction of the Cu(110) surface. Partially oxidizing the Cu(110) surface results in striped domains along the [001] direction consisting of O–Cu–O chains within every other interstitial lattice site in the [1-10] direction, which is referred to as Cu(110)-(2 × 1)O added-row (AR) reconstruction.^{24,25} Figure 1B shows an overview NC-AFM image with two copper oxide stripes (brighter domains). The blue square marks the area where the high-resolution image in Figure 1C was recorded and which is centered around a defect at the end of one of the added rows. Besides atomic resolution within the oxide domain, this image also displays atomic corrugation on the Cu metal domain, where the maxima in the contrast are assigned to the positions of the Cu atoms. The Cu rows in the [110] direction are marked by two black dashed lines. Taking into consideration the structure depicted in Figure 1A, to follow these dashed lines toward the oxide domain allows to directly assign the dark features in the oxide domain to the position of the oxygen atoms. Consequently, the bright protrusions are the copper atoms within the added rows. We also observe atomic corrugation of a few picoamperes in the simultaneously recorded tunneling current image. However, this image showed an inverted contrast to the NC-AFM topography channel, which strongly suggests that it is dominated by feedback-induced cross-talk.²⁶ Therefore, after the NC-AFM image in Figure 1C, we recorded an image in pure STM mode (Figure 1D). Subsequently, another NC-AFM image with identical settings to the previous one (Figure 1C) was recorded. By comparing the two NC-AFM images, we do not find any noticeable lateral drift between tip and sample (Figure S1). Therefore, the contrast features in the NC-AFM and STM images in Figure 1C and D correspond to the same

area and can directly be compared. The blue grid lines in both images indicate the position of the Cu atoms within the added rows as recorded by NC-AFM. Although we can exclude lateral drift, the bright rows in the two images show a significant offset of $\delta = 2.80 \pm 0.15 \text{ \AA}$ in the [110] direction, which will be analyzed in detail below.

The NC-AFM images in Figure 1B and C reflect planes of constant frequency shift where an in-depth physical analysis is difficult. To obtain information about possible distance-dependent contrast changes and to quantitatively assess the force interaction within the tip–sample junction, a complete 3D-AFM data set in the layer-by-layer approach was recorded on the area in Figure 1C. This method provides the complete (3D) force field as experienced by the tip in this area.^{27–29} Figure 2A–D shows resulting horizontal force cuts (force at constant height) at different z distances. The z -values refer to the point of closest tip–sample approach, which is located at the defect. White areas indicate sites where no experimental z -values are available due to the large topographical corrugation. Figure 2E displays a vertical force cut along one of the added rows as indicated in Figure 2C. The force–distance curves in Figure 2F correspond to the location of a Cu atom and an O atom within the added row (AR-Cu, AR-O) as indicated by vertical gray dashed lines in Figure 2E. While the force–distance curves show a short-range region with atomic contrast restricted to $z \leq 2 \text{ \AA}$, there is a significant contribution of long-range forces extending several nanometers from the closest tip approach.

To obtain a detailed atomistic understanding about the tip–sample interactions behind the data presented in Figure 2A–F, we simulated force–distance curves using DFT. Prior to recording the experimental data, stable imaging conditions were obtained by indentations of the tip into the oxide domains of the surface. Therefore, we expect the tip apex to be covered with sample material and focused on stable Cu(111)-based tetragonal tip models that terminate in a copper or an oxygen atom (Figure 2G). These two tips were found to widely describe the NC-AFM (and STM) imaging characteristics on copper oxide surfaces.^{30–33} Furthermore, we considered an OH-terminated tip and a Cu tip where an O atom is bound to one of its side faces (Cu-CuO tip) as shown in Figure S2A. We employed these model tips to compute force–distance curves above the AR-O and AR-Cu sites, which are presented in Figure 2H and Figure S2B. To remove inherent uncertainties that arise from long-range force contributions in the measured data, we determined the difference between the AR-Cu and AR-O force curves ($F_{\text{AR-Cu}} - F_{\text{AR-O}}$). Figure 2I displays the comparison of the theoretical and experimental difference curves obtained in this manner. As the absolute tip–sample distance in the experiment is unknown, the experimental data were shifted along the z -axis to find the best fit with simulations. We find good agreement with the experiment for the oxygen-terminated probe, with a closest approach above the AR-O atom of $d_{\text{AR-O}}^{\text{min}} = 3.4 \text{ \AA}$.

The force–distance curves in Figure 2H are in line with a more general trend of the considered tips with regard to other O-reconstructed copper surfaces. Independent of the tip–sample distance in all reported cases, the O-terminated Cu tip images the surface Cu atoms and exhibits a significantly reduced overall force interaction as compared to the pure metallic probe.^{30–33} The weak interaction of the O-terminated tip suggests that the oxygen atom chemically passivates this probe. In contrast, the pure Cu tip exhibits a stronger

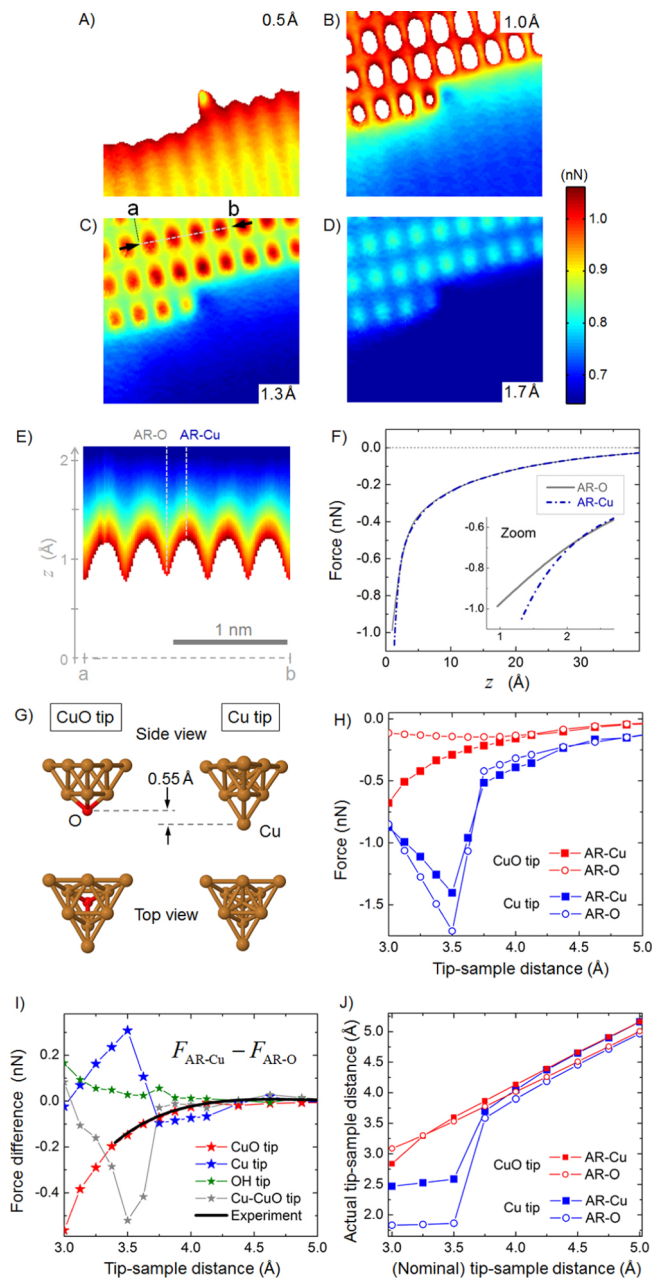


Figure 2. (A–D) Horizontal force cuts ($2.93 \times 2.78 \text{ nm}^2$) of the 3D NC-AFM data set. The tip–sample distance (z) is given with respect to the lowest point located at the central defect. (E) Vertical force cut (same color scale as in A–D), corresponding to the distance ab as depicted in C. (F) Force–distance curves acquired above an AR-O and an AR-Cu atom as indicated by the gray lines along the z -axis in the vertical force cut in E. It should be noted that in the actual force calculation $\Delta f(z)$ values back to 6 nm covering the regime of free oscillation were considered. (G) Cu-based model tips terminated by an O atom (CuO tip) and a Cu atom (Cu tip). (H) Calculated force–distance curves for the CuO and Cu tip above an AR-O and AR-Cu atom of the surface. (I) Comparison of theoretical and experimental difference curves for the considered model tips, clearly showing that in the experiment the tip was O-terminated. (J) Nominal versus actual tip–sample distance for the two tip structures, revealing pronounced structural relaxations only for the Cu tip.

interaction with the surface, as well as discontinuities in the force–distance curves in the range between 3.5 and 4.0 \AA

(Figure 2H). By analyzing discrepancies between nominal and actual tip–sample distances presented in Figure 2J, we relate the discontinuities with atomic relaxations within the tip–sample junction. The Cu-terminated tip deforms at close approach to the surface, whereas the O-terminated tip remains structurally stable. These findings explain why the tip configuration with the terminal O atom is identified most frequently when imaging copper oxide surfaces with NC-AFM or STM.^{31,33} Owing to its higher chemical reactivity and the tendency for atomic relaxations within the tip–sample junction, the pure Cu tip is easily contaminated by oxygen in the experiments.³¹

We combined DFT with NEGF conductance calculations to explore the STM contrast mechanisms on the Cu(110)-(2 × 1) O reconstruction for the pure Cu- and O-terminated tip. Figure 3 features STM images computed at various tip–sample

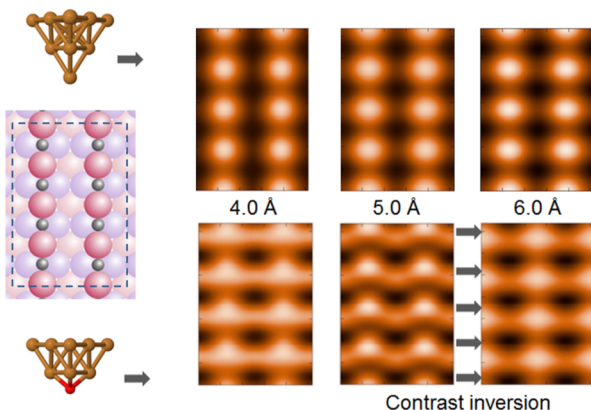


Figure 3. STM contrast calculations of the Cu(110)-(2 × 1)O reconstruction simulated for a bias voltage of $U_{\text{gap}} = 0.1$ V (as used in the experimental image in Figure 1) at different tip–sample distances for the pure Cu tip (first row) and the O-terminated tip (second row). The structural models of the surface and tips are shown on the very left side.

distances, with the same bias voltage as used for the recording of the experimental image in Figure 1D (0.1 V). The imaging characteristics of the pure metallic tip exhibit maxima located on the AR-Cu sites and no variation with tip–sample distance. The O-terminated tip shows more complex contrasts, asymmetric features, and changes with the tip–sample distance. In particular, we observe a contrast inversion in the tip–sample distance range of 5.0–6.0 Å, with added row current maxima at low scanning heights shifting to spaces between added rows when the tip–sample distance is increased. The effect can be explained by the varying distance dependence of the current signal contributions from the apex O atom and the Cu atoms of the second (triangular) layer of the tip, as previously found in the study of the oxygen-induced $(2\sqrt{2} \times \sqrt{2})R45^\circ$ reconstruction on the Cu(100) surface.³¹ The simulated images for the O-terminated tip at large tip–sample distances describe well the experimental STM contrast explaining the apparent pronounced offset of the current maxima between the experimental NC-AFM and STM images in Figure 1C and D. Since the STM contrast study supplies an independent means of tip chemistry identification, the good agreement found between theoretical and experimental data further validates our earlier finding that the data presented in Figures 1 and 2 were collected with an O-terminated Cu tip. Therefore, the NC-AFM and STM contrast signatures obtained on an oxide

domain boundary as in Figure 1C and D can be used as fingerprints for an O-terminated Cu tip.

As mentioned earlier, the mechanism leading to high-resolution NC-AFM images of organic molecules is believed to be closely related to the dynamic lateral deflection of the probe particle during scanning.^{21,34} In contrast, for the case of the O-terminated Cu tip as characterized in the present study, the rigid tetrahedral configuration of the covalently bound terminal O atom would probably not allow significant lateral displacements during scanning. Furthermore, its generally low force interaction with the surface can be expected to facilitate imaging at small tip–sample distances. To test this tip as a probe for imaging a flat organic molecule adsorbed on a surface, we initiated further experiments where we prepared a sample with the striped (2 × 1)-reconstructed oxide domains on Cu(110) and subsequently deposited DCLN molecules (see structure in Figure 4A). The DCLN molecules adsorb exclusively on the pure metal domains, as previously found for other organic compounds on this nanostructured surface.^{35,36} Tip functionalization with an O-terminated Cu tip is achieved by a procedure where in the last step the tip is slightly indented in one of the oxide domains (see Methods section for details). It is pointed out that this procedure is not equivalent to directly picking up a single O atom from an oxide domain. Any attempts to achieve this remained unsuccessful, which we attribute to the strong chemical bonding configuration within the added row reconstruction. Rather, the final tip indentations lead to the transfer of a cluster of O and Cu atoms to the apex³³ or the structural rearrangement of an existing cluster at the tip.^{16,17} Subsequently obtained NC-AFM and STM contrasts from an oxide domain boundary are then compared with the contrast signatures discussed for the data in Figure 1, which are used as tip fingerprints for an O-terminated Cu tip, similar to previously proposed approaches.^{33,37} In agreement with studies on the O-induced Cu(110) $c(6 \times 2)$ and Cu(100) $(2\sqrt{2} \times \sqrt{2})R45^\circ$ reconstructions, we find that this way an O-terminated Cu tip can be obtained with high reproducibility.^{31,33}

After successful tip functionalization with an O-terminated Cu tip we imaged a single DCLN molecule adsorbed on the pure metal domain in constant-height NC-AFM. Figure 4B presents a frequency shift image recorded after the tip was approached by 0.6 Å from a reference tip–sample distance corresponding to a STM set-point of $I = 30$ pA at $U_{\text{gap}} = 0.1$ V above the pure Cu domain. The intramolecular structure of the DCLN featuring the internal bonds is clearly resolved in this image. The fact that such a good resolution can be achieved with the O-terminated Cu tip raises the question of the exact imaging mechanism in this case. Therefore, we recorded site-specific force–distance curves, which are shown in Figure 4C. Here $z = 0$ refers to the plane of constant height where the image in Figure 4B was recorded. The three force–distance curves recorded on the inner parts of the molecule corresponding to the center (blue), inner C–C bond (black), and hollow site (green) of the DCLN reveal that the internal bond structure can be resolved only in the distance regime to the left of the force minimum. In contrast, the force curve recorded on the location of an outer C–C bond of the DCLN (red) exhibits a force minimum around 0.2 nN higher and the lowest force interaction at $z = 0$ Å as compared to the other force–distance curves. This reflects the more pronounced Δf contrast observed at the outer bonds of the molecule, in

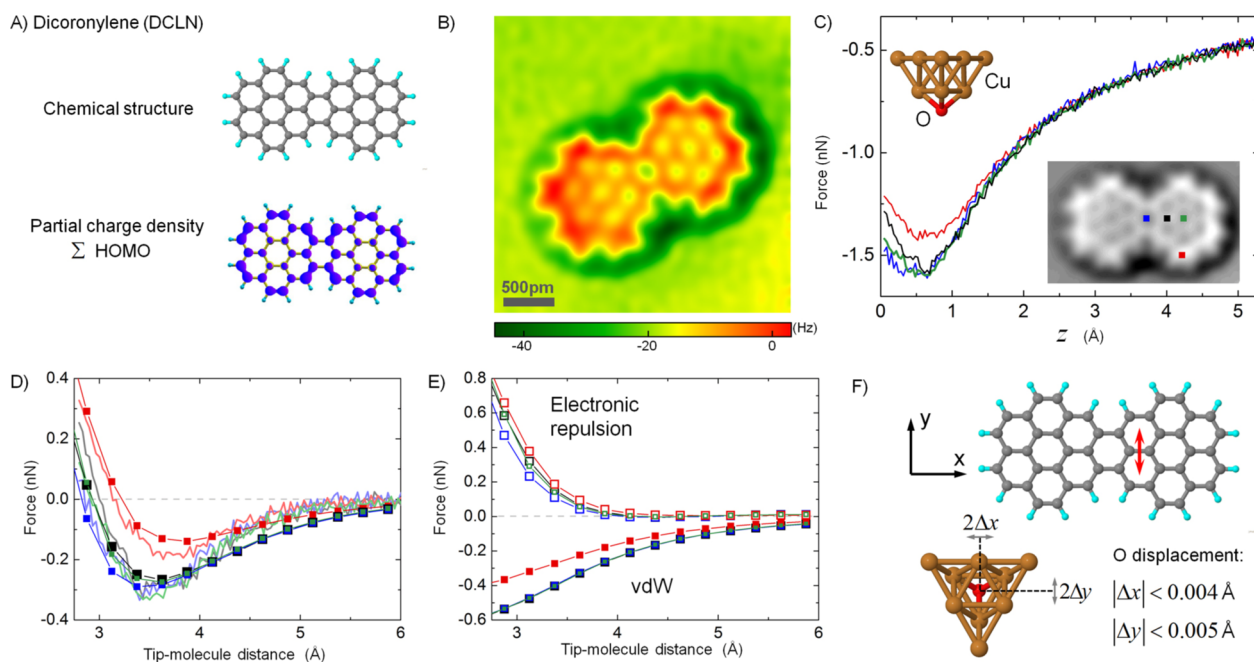


Figure 4. (A) Structural model and partial charge density of the last occupied molecular orbitals (HOMO + HOMO1 + HOMO2) shown for an isovalue Iv of 0.008 for DCLN. (B) Constant-height frequency shift image recorded on a single DCLN adsorbed on Cu(110) with an O-terminated Cu tip. (C) Experimental force–distance curves recorded on the DCLN, where $z = 0$ corresponds to the constant-height plane in B. The lateral position where the data were recorded is marked as an inset. (D) Comparison of experimental and simulated force–distance curves in the short-range regime. From the experimental curves, a vdW background was subtracted for better comparability. In addition, the experimental curves were shifted along the z -axis by 2.80 Å to fit the simulation. (E) Simulated data from D with separated force contributions: electronic repulsion and vdW forces. (F) Schematic representation of a simulated line scan calculated along the red arrow, which crosses the C–C bond corresponding to the site of the black force–distance curve in C–E. Eleven data points were calculated along the red arrow at a tip–sample distance of 2.80 Å.

agreement with previous work utilizing CO-functionalized tips.^{7,38}

To understand the intramolecular contrast formation mechanisms with an O-terminated Cu tip in more detail, we performed DFT+vdW-D3 simulations approaching the tip to the isolated molecule on the same sites as in the experiment. To facilitate the comparison with the experiment, a sphere-plane van der Waals (vdW) function was subtracted from the measured force–distance curves. This allows the direct comparison of the experimental and simulated force interaction, which shows excellent qualitative and quantitative agreement (Figure 4D). By fitting the z -scale of the experimental data to the simulation, we obtain an absolute tip–molecule distance of 2.80 Å, at which intramolecular resolution is achieved. Knowing the distance regime in which the O-terminated Cu tip shows intramolecular resolution allows now to check if the presumption of a rigidly connected O atom at the tip apex at such small tip–surface distances is valid. Therefore, to analyze possible lateral relaxations of the O atom at the tip apex during data acquisition, we simulated lateral scans at the same distance where the image was recorded. We started the scan at a tip–sample distance of 2.80 Å from the center of a hollow site of the DCLN molecule, crossed an inner C–C bond, and finished the scan in the center of another hollow site (see schematic in Figure 4F). During this simulation the bottom two layers of the tip were allowed to relax, and we determined the position of the tip-terminating oxygen atom along the scan. In all cases the absolute lateral deflection in x - and y -direction of the O atom was as low as $|\Delta x| \leq 0.4$ pm and $|\Delta y| \leq 0.5$ pm relative to its optimum position. Compared to the values determined for a CO molecule,⁷ these values are about 2 orders of magnitude

smaller and can be neglected as a major factor for the imaging mechanism.

As mentioned above, previous work with CO-functionalized tips for high-resolution imaging of organic molecules showed a pronounced systematic overestimation of bond lengths of up to 30%, which can be assigned to the flexibility of the CO molecule at the tip.^{7,20,34,39} Also for Xe-functionalized tips, lateral relaxations seem to play a crucial role explaining the intramolecular imaging mechanism.⁴⁰ Being now able to exclude significant effects due to lateral tip relaxations during the recording of our data leads us to an evaluation of bond lengths in the constant-height NC-AFM image in Figure 4B. Due to the increased interaction of the outermost C–C bonds of the molecule, this evaluation is difficult. Therefore, we restricted the experimental bond length determination to the internal ones. From the structural optimization of the free molecule we obtained a theoretical value of 1.43 Å for these bonds (Figure S3). The corresponding experimental bond lengths were found to be 1.45 ± 0.23 Å (Figure S4). Although we do not obtain a systematic overestimation of bond lengths from the experiment as is the case for CO-functionalized tips, the uncertainty of about 16% is significant. This mainly arises from the broad bond structure observed in our contrast, which in turn is probably a consequence of the rigidity of our tip. On the other side, a flexible tip apex leads to an apparent sharpening of the bonds but also to their mentioned artificial elongation.^{7,22,34}

In the following, based on the good agreement between experimental and simulated force–distance curves in Figure 4D, the contrast obtained with the O-terminated Cu tip is analyzed in more detail. To facilitate this analysis, the

contribution of the microscopic vdW interaction to the simulated total force values in Figure 4D was extracted and plotted separately (Figure 4E). The remaining forces (difference of total and vdW forces) contain the repulsive components, including the short-range electrostatic interaction as well as Pauli repulsion, and are labeled electronic repulsion in Figure 4E. In agreement with a previous first-principles study by Ondráček *et al.*,⁴¹ this reveals that for the internal bonds (blue, black, and green curves) the attractive vdW components are almost identical and do not contribute to the contrast. In this case the intramolecular contrast is solely described by the electronic repulsion between the tip and the intramolecular bonding structure.

Theoretical work by Sang *et al.* suggested that the high resolution achieved in such NC-AFM experiments is based on an inhomogeneous charge distribution at the tip termination, where negatively charged tips seem to produce the clearest intramolecular contrast due to the increased repulsive interaction on electron-rich sites.³⁷ In fact, considering the various probe particles, which provide good image contrast (CO, Cl, Xe, Br, or O-terminated organic molecules),^{2,13,23} the correlation between (atomic) electronegativity of the terminating tip atom and high-quality submolecular imaging properties seems to be a general and important aspect (Table S1). Therefore, it appears that for the O-terminated Cu tip as studied here, besides its chemical and structural stability, a major ingredient for the good performance in our constant-height experiment on DCLN is the high atomic electronegativity of oxygen and a related increased electron density at the tip apex.

Moving on to the discussion about the contrast in the case of the outer C–C bonds (red curve in Figure 4E), we observe both an increased electronic repulsion and a less attractive vdW contribution explaining the increased Δf contrast on these sites. This confirms a previous suggestion where a similar effect was observed for CO-functionalized tips.⁷ The less attractive vdW contribution takes account of the reduced vdW forces at the periphery of the DCLN, whereas the larger repulsion above the outer C–C bonds in turn can be explained by a larger charge density in these bonds. The latter is reflected in an increased partial charge density associated with the last occupied molecular orbital in these bonds as shown in Figure 4A (see also plots of the total charge density at different isovalue and effects on bond lengths in Figures S5 and S3). Quantifying the simulated force contributions at the outer bonds with respect to the inner ones reveals an overall force contrast (red curve minus black curve) at the minimum tip–sample distance of about 0.24 nN, of which 70% accounts for the vdW and 30% for the component of electronic repulsion, respectively.

Here it is pointed out that the reduced vdW contribution at the outer bonds leads to a distinct force contrast even in the attractive regime (Figure 4D and E). This provides promising perspectives for cases where organic molecules are only weakly adsorbed on a surface and, as a consequence, are spatially manipulated by the strong forces when approaching the repulsive regime. We were confronted with such a problem when we performed constant height experiments of DCLN molecules adsorbed on the oxygen-induced $(2\sqrt{2} \times \sqrt{2})R45^\circ$ missing row reconstruction of the Cu(100) surface. Nevertheless, we were able to visualize the outer bond structure of the DCLN in this case just before the molecule was displaced (Figure S6). This could be a promising approach also for other metal oxide substrates, where organic molecules tend to adsorb

weakly.⁴² Nevertheless, there is a high technological relevance to the related interfaces. In such cases, a distinct contrast of the outer bond structure obtained already in the attractive regime in NC-AFM experiments could provide important insights for the bottom-up synthesis of molecular architectures obtained by self-assembly or on-surface chemical reactions.^{43,44}

CONCLUSIONS

The oxygen-termination of the investigated tip results in a weak force interaction within the tip–sample junction, which can be interpreted as a chemical passivation of this probe. At the same time this tip shows a high structural stability as compared to a pure Cu tip. These properties are probably the reason that this tip structure is most frequently found when oxidized Cu surfaces are imaged by STM or NC-AFM. Here we explored NC-AFM and STM contrasts on a partly oxidized Cu(110) surface with striped (2×1) -O reconstructed nanodomains. By DFT simulations, we determined NC-AFM and STM contrast signatures, which allowed the unambiguous identification of this tip-termination. Furthermore, we demonstrated the capabilities of this tip to image a planar organic molecule adsorbed on Cu(110) in the repulsive regime, revealing its internal bond structure. From simulated line scans across a C–C bond, we show that tip flexibility can be neglected in the contrast mechanism and that this is not an ultimate requirement for high-resolution imaging in the repulsive regime. On the other side, as pointed out by Gross *et al.*, the apparent bond sharpening due to the flexibility of a CO molecule at the tip apex is important to measure small bond-distance variations on the cost of the corresponding (overestimated) absolute values.⁷ Due to the broadened intramolecular bond structure as imaged by the O-terminated Cu tip, which is a result of its rigidity, such small variations are not accessible. However, it does not show a systematic overestimation of absolute bond lengths.

Being able to exclude tip flexibility as an ultimate necessity for high-resolution imaging facilitates a detailed discussion about the fundamental imaging mechanism in NC-AFM experiments performed in the repulsive regime. Our combined analysis of experimental and simulated force–distance curves reveals that for the inner bonds of the molecule electronic repulsion is the dominant interaction at small tip–sample distances ($d \leq 3.5 \text{ \AA}$). It is suggested that in this regime the increased electronic repulsion above the bonds and the resulting intramolecular contrast are a consequence of the high atomic electronegativity of oxygen and the related increased electron density at the apex of the O-terminated Cu tip.

Opposed to the inner bonds, the outer ones exhibit both an increased electronic repulsion and a reduced vdW interaction. On the basis of our simulations, we find that the observed increased Δf contrast at the outer bonds is dominated by the reduced vdW interaction with a fraction of 70%, but with a considerable part (30%) related to an increased charge density in these bonds. Due to the reduced vdW interaction at the outer bonds, these can be imaged even in the attractive regime of the tip–sample junction. This observation could be particularly interesting for sample systems where molecules are only weakly adsorbed on a substrate and hence do not allow imaging in the repulsive regime. This provides interesting perspectives for experiments on bulk metal oxides and substrate systems with oxygen-induced reconstructions, where tip passivation by an oxygen termination could be achieved. Such

a perspective is particularly promising due to the high technological relevance of nanostructures and interfaces involving metal oxides and organic layers.

METHODS

Theory. DFT simulations were carried out with the OpenMX code,⁴⁵ norm-conserving ultrasoft pseudopotentials, PBE functional, and double- ζ pseudoatomic orbitals extending to 6 au. The Cu(110) and oxidized Cu(110)-(2 \times 1)O surfaces were simulated in a four-layer Cu slab geometry with a 2 \times 1 Cu(110) unit cell of dimensions 5.2 \times 3.7 Å². With two bottom layers fixed to bulk geometry (lattice constant of 3.619 Å), the positions of the remaining atoms were optimized in calculations with an energy cutoff of 400 Ry and 8 \times 12 \times 1 k -point mesh. Force tolerance adopted throughout this work is 10⁻⁴ au. Geometry analysis of the oxide AR reconstruction revealed that surface-topping O atoms are positioned 0.15 Å above the plane of AR-Cu atoms, in line with earlier predictions.⁴⁶ Three-layer Cu(111) clusters terminating in oxygen or copper atoms were employed as NC-AFM probes. Furthermore, complementary Cu apexes with an O atom bound to one of the side faces and an OH termination were considered.

Hamilton matrices for the surface were combined with the tip electronic structure and long-range tip–surface hopping probabilities (extracted from local-orbital DFT calculations) and used as input for the in-house STMAD code to compute tip–sample conductance and currents.^{47,48} Stable tip configurations were placed above the surface, with tip–sample distance d defined as the height difference between the tip apex atom and the highest feature of the oxide surface (AR-O atom). The tunneling current was integrated in 0.05 eV bins, while only dominant current contributions from the bottom two tip layers into the atoms in the uppermost Cu layer and the oxide added row were included. Tips were translated laterally across the surface to compute two-dimensional STM surface images.

Surface area was expanded to 6 \times 4 Cu(110)-(2 \times 1)O unit cells (15.4 \times 14.5 Å²) for NC-AFM simulations featuring a 2 \times 2 \times 1 k -point grid. Tips were initially placed at a distance of $d = 5$ Å above different surface sites and lowered in steps of 0.25 Å to simulate force–distance curves. At each height, the upper layers of the surface and the two lower layers of the tip were optimized to allow for structural rearrangements, and the tip–surface interaction energy was determined. Forces were extracted by differentiating the total energy and directly from the total force acting within the tip–sample junction. Following the structural optimization of the isolated DCLN molecule (Gamma point k -space sampling), atomic coordinates were kept fixed within a two-dimensional plane to mimic its interaction with the substrate during NC-AFM simulations. Force–distance curves were computed by lowering the tip as before and including vdW DFT-D3 and basis set superposition error (BSSE) corrections to the total energy, as implemented in the OpenMX code. The lateral NC-AFM scan was conducted by displacing the tip between two internal hollow sites on DCLN sites in 11 steps, then tracing back over the trajectory to rule out dissipative effects. Lower layers of the tip were optimized throughout, allowing one to monitor any lateral displacements of the tip-terminating O atom. Prior to comparison with theory, the long-range contribution of the experimental force–distance curves was fitted to the sphere–plane vdW interaction model $F = C/(z - z_0)^2$ ($C = 57.4708$ nN·Å² and $z_0 = -6.059\ 06$ Å) and subtracted from the total force data to obtain the experimental short-range contribution. When compared with theoretical results, experimental curves were translated along the z -axis to align the position of the first minimum of the interaction force recorded upon tip approach, revealing the distance of closest tip approach above the molecule to be 2.8 Å.

Experiments. The NC-AFM measurements were performed with a low-temperature scanning probe microscope (LT-STM/AFM) from Omicron Nanotechnology, which is operated under ultra-high-vacuum conditions and at liquid helium temperatures ($T \approx 5$ K). A tuning fork based cantilever in the qPlus configuration with an electrochemically etched W tip in the frequency modulation mode was used.⁴⁹ The spring constant of the qPlus sensor is $k \approx 2000$ N m⁻¹, and its

resonance frequency around 22 kHz. Typical quality factors are in a range $Q = 30\ 000$ –50 000 at liquid He temperatures. The oscillation amplitudes in the measurements were 6.0 Å for the 3D NC-AFM and 0.9 Å for the constant-height experiments, respectively. In the presented experiments, we observed no notable energy dissipation within the data.

The 3D NC-AFM data set was recorded by the layer-by-layer approach with active feedback loop. Data acquisition in constant-height mode is problematic in the present case due to the high corrugation at the oxide domain boundary. Moreover, force spectroscopy on a fine, equally spaced grid is disfavored due to related drift and piezocreep effects. A detailed comparison of these different techniques to record a 3D NC-AFM data set is given by Baykara *et al.*²⁹ Our data set encompasses the frequency shift (Δf) and topography (z) data of 47 NC-AFM images recorded with Δf set-points ranging from −6.0 to −1.5 Hz, covering the regime of the short-range forces. The 47 images were recorded on an area of 3 \times 3 nm² and with 180 \times 180 pixels, which took about 3 h. During this recording time, tip–sample drift was linear: 64 pm/h in the x - and 16 pm/h in the y -direction. Postacquisition drift correction reduced the data set to 167 \times 176 pixels. After adding the long-range part of a $\Delta f(z)$ curve (up to 6 nm) to each pixel,^{27,28} the data set was converted to forces applying the Sader–Jarvis algorithm.⁵⁰

For the sample preparation a Cu(110) single crystal was cleaned by repeated cycles of Ar⁺ sputtering (2 keV) and annealing ($T \approx 700$ K). After the last annealing cycle, the sample was exposed to molecular oxygen in a pressure range of (2–4) $\times 10^{-8}$ mbar for 30 s (3D NC-AFM) or 10 s (constant-height measurements) with the sample kept at $T \approx 500$ K. Subsequently, another annealing cycle was performed before the sample was transferred to the microscopy stage. For the constant-height experiment, in addition to the partial (2 \times 1) oxidation, diconorylene (benzo[10,11]phenanthro[2',3',4',5',6':4,5,6,7]chrysene[1,2,3-bc]coronene) was deposited on the sample from a quartz crucible of a Knudsen cell, which was heated up to 645 K. The sample surface was exposed to the molecular beam for 90 s, while the sample was kept at room temperature.

While the tip preparation procedures prior to the recording of the 3D NC-AFM data were performed by a combination of voltage pulses and indentations in an oxide domain, for the constant-height experiments we followed a more controlled approach. First, to reduce long-range force contributions, a reasonably sharp tip apex on a mesoscopic scale was created by indentations of several nanometers into the surface. This was realized by (slow) indentations between 2 and 10 nm at a ramp speed of ~ 0.2 –1.0 nm s⁻¹ in STM mode without any qPlus oscillation. We usually started these indentations from a reference tip–sample distance corresponding to an STM set-point of about 100 mV/0.5 nA. Subsequently, the tip was retracted by at least 20 nm and reapproached on a clean Cu domain nearby. To estimate the (mesoscopic) sharpness of the resulting tip structure, this reapproach was performed with an oscillating tip at active STM-feedback settings (100 mV/0.5 nA). From the measured frequency shift, the sharpness of the tip can be estimated. Only tips with -4 Hz $\leq \Delta f \leq -12$ Hz were considered for further tip functionalization toward the desired O-termination. This was accomplished by repeated soft indentations of only a few angstroms in one of the copper oxide domains until stable imaging conditions were obtained. To subsequently obtain a tip fingerprint, we switched to NC-AFM and approached one of the oxide domain boundaries in constant frequency shift mode. By lowering the Δf set-point, the tip–sample distance was reduced until atomic corrugation on both the oxide and the metal domain was obtained, clearly showing the copper atoms in the oxide as topographical maxima. As discussed in the **Results and Discussion** section, switching back to STM imaging without tip oscillation on the same scan area provides additional indicators for successful tip functionalization with a terminating O atom. The NC-AFM and STM images recorded as tip fingerprint prior to the recording of the constant-height data on the DCLN are shown in Figure S7.

ASSOCIATED CONTENT**Supporting Information**

The Supporting Information is available free of charge on the ACS Publications website at DOI: [10.1021/acsnano.5b06513](https://doi.org/10.1021/acsnano.5b06513).

Additional figures and a table ([PDF](#))

AUTHOR INFORMATION**Corresponding Author**

*E-mail: harry.moenig@uni-muenster.de.

Author Contributions

^{II}D. R. Hermoso and O. Díaz Arado contributed equally to this work.

Notes

The authors declare no competing financial interest.

ACKNOWLEDGMENTS

Financial support from the Deutsche Forschungsgemeinschaft (DFG) through the transregional collaborative research center (TRR 61, project B7) and from the Spanish Ministry of Economy and Competitiveness MINECO through projects MAT2011-023627, CSD2010-00024 and MAT2014-54484-P is gratefully acknowledged. Access to the Magerit Supercomputer (CesViMa, Madrid) was provided through the Spanish Supercomputing Network (RES, Spain). The COST Action CM1104 is gratefully acknowledged.

REFERENCES

- (1) Morita, S.; Wiesendanger, R.; Meyer, E., Eds. *Noncontact Atomic Force Microscopy; NanoScience and Technology*; Springer-Verlag: Berlin Heidelberg, 2002; pp 1–440.
- (2) Gross, L.; Mohn, F.; Moll, N.; Liljeroth, P.; Meyer, G. The Chemical Structure of a Molecule Resolved by Atomic Force Microscopy. *Science* **2009**, *325*, 1110–1114.
- (3) Mohn, F.; Gross, L.; Moll, N.; Meyer, G. Imaging the Charge Distribution within a Single Molecule. *Nat. Nanotechnol.* **2012**, *7*, 227–231.
- (4) Schuler, B.; Liu, S.-X.; Geng, Y.; Decurtins, S.; Meyer, G.; Gross, L. Contrast Formation in Kelvin Probe Force Microscopy of Single π -Conjugated Molecules. *Nano Lett.* **2014**, *14*, 3342–3346.
- (5) Kocić, N.; Weiderer, P.; Keller, S.; Decurtins, S.; Liu, S.-X.; Repp, J. Periodic Charging of Individual Molecules Coupled to the Motion of an Atomic Force Microscopy Tip. *Nano Lett.* **2015**, *15*, 4406–4411.
- (6) Albrecht, F.; Repp, J.; Fleischmann, M.; Scheer, M.; Ondráček, M.; Jelínek, P. Probing Charges on the Atomic Scale by Means of Atomic Force Microscopy. *Phys. Rev. Lett.* **2015**, *115*, 076101.
- (7) Gross, L.; Mohn, F.; Moll, N.; Schuler, B.; Criado, A.; Guitián, E.; Pena, D.; Gourdon, A.; Meyer, G. Bond-Order Discrimination by Atomic Force Microscopy. *Science* **2012**, *337*, 1326–1329.
- (8) Schuler, B.; Meyer, G.; Pena, D.; Mullins, O. C.; Gross, L. Unraveling the Molecular Structures of Asphaltenes by Atomic Force Microscopy. *J. Am. Chem. Soc.* **2015**, *137*, 9870–9876.
- (9) Moreno, C.; Stetsovych, O.; Shimizu, T. K.; Custance, O. Imaging Three-Dimensional Surface Objects with Submolecular Resolution by Atomic Force Microscopy. *Nano Lett.* **2015**, *15*, 2257–2262.
- (10) Pawlak, R.; Kawai, S.; Fremy, S.; Glatzel, T.; Meyer, E. Atomic-Scale Mechanical Properties of Oriented C₆₀ Molecules Revealed by Noncontact Atomic Force Microscopy. *ACS Nano* **2011**, *5*, 6349–6354.
- (11) Zhang, J.; Chen, P.; Yuan, B.; Ji, W.; Cheng, Z.; Qiu, X. Real-Space Identification of Intermolecular Bonding with Atomic Force Microscopy. *Science* **2013**, *342*, 611–614.
- (12) Kawai, S.; Sadeghi, A.; Feng, X.; Lifen, P.; Pawlak, R.; Glatzel, T.; Willand, A.; Orita, A.; Otera, J.; Goedecker, S.; et al. Obtaining Detailed Structural Information about Supramolecular Systems on Surfaces by Combining High-Resolution Force Microscopy with *ab Initio* Calculations. *ACS Nano* **2013**, *7*, 9098–9105.
- (13) Sweetman, A. M.; Jarvis, S. P.; Sang, H.; Lekkas, I.; Rahe, P.; Wang, Y.; Wang, J.; Champness, N.; Kantorovich, L.; Moriarty, P. Mapping the Force Field of a Hydrogen-Bonded Assembly. *Nat. Commun.* **2014**, *5*, 1–7.
- (14) Riss, A.; Wickenburg, S.; Gorman, P.; Tan, L. Z.; Tsai, H.-Z.; de Oteyza, D. G.; Chen, Y.-C.; Bradley, A. J.; Ugeda, M. M.; Etkin, G.; et al. Local Electronic and Chemical Structure of Oligo-Acetylene Derivatives Formed Through Radical Cyclizations at a Surface. *Nano Lett.* **2014**, *14*, 2251–2255.
- (15) Albrecht, F.; Pavlicek, N.; Herranz-Lancho, C.; Ruben, M.; Repp, J. Characterization of a Surface Reaction by Means of Atomic Force Microscopy. *J. Am. Chem. Soc.* **2015**, *137*, 7424–7428.
- (16) Welker, J.; Weymouth, A. J.; Giessibl, F. J. The Influence of Chemical Bonding Configuration on Atomic Identification by Force Spectroscopy. *ACS Nano* **2013**, *7*, 7377–7382.
- (17) Hofmann, T.; Pielmeier, F.; Giessibl, F. J. Chemical and Crystallographic Characterization of the Tip Apex in Scanning Probe Microscopy. *Phys. Rev. Lett.* **2014**, *112*, 066101.
- (18) Sun, Z.; Boneschanscher, M. P.; Swart, I.; Vanmaekelbergh, D.; Liljeroth, P. Quantitative Atomic Force Microscopy with Carbon Monoxide Terminated Tips. *Phys. Rev. Lett.* **2011**, *106*, 046104.
- (19) Emmrich, M.; Huber, F.; Pielmeier, F.; Welker, J.; Hofmann, T.; Schneiderbauer, M.; Meuer, D.; Polesya, S.; Mankovsky, S.; Ködderitzsch, D.; et al. Subatomic Resolution Force Microscopy Reveals Internal Structure and Adsorption Sites of Small Iron Clusters. *Science* **2015**, *348*, 308–311.
- (20) Moll, N.; Schuler, B.; Kawai, S.; Xu, F.; Peng, L.; Orita, A.; Otera, J.; Curioni, A.; Neu, M.; Repp, J.; et al. Image Distortions of a Partially Fluorinated Hydrocarbon Molecule in Atomic Force Microscopy with Carbon Monoxide Terminated Tips. *Nano Lett.* **2014**, *14*, 6127–6131.
- (21) Hapala, P.; Kichin, G.; Wagner, C.; Tautz, F. S.; Temirov, R.; Jelínek, P. Mechanism of High-Resolution STM/AFM Imaging with Functionalized Tips. *Phys. Rev. B: Condens. Matter Mater. Phys.* **2014**, *90*, 085421.
- (22) Hämäläinen, S. K.; van der Heijden, N.; van der Lit, J.; den Hartog, S.; Liljeroth, P.; Swart, I. Intermolecular Contrast in Atomic Force Microscopy Images without Intermolecular Bonds. *Phys. Rev. Lett.* **2014**, *113*, 186102.
- (23) Mohn, F.; Schuler, B.; Gross, L.; Meyer, G. Different Tips for High-Resolution Atomic Force Microscopy and Scanning Tunneling Microscopy of Single Molecules. *Appl. Phys. Lett.* **2013**, *102*, 073109.
- (24) Kern, K.; Niehus, H.; Schatz, A.; Zeppenfeld, P.; Goerge, J.; Comsa, G. Long-Range Spatial Self-Organization in the Adsorbate-Induced Restructuring of Surfaces: Cu100-(2 × 1)O. *Phys. Rev. Lett.* **1991**, *67*, 855–858.
- (25) Coulman, D. J.; Wintterlin, J.; Behm, R. J.; Ertl, G. Novel Mechanism for the Formation of Chemisorption Phases: The (2 × 1)O-Cu(110) “Added Row” Reconstruction. *Phys. Rev. Lett.* **1990**, *64*, 1761–1764.
- (26) Baykara, M. Z.; Todorovic, M.; Möning, H.; Schwendemann, T. C.; Rodrigo, L.; Altman, E. I.; Pérez, R.; Schwarz, U. D. Simultaneous Measurement of Multiple Independent Atomic-Scale Interactions Using Scanning Probe Microscopy: Data Interpretation and the Effect of Cross-Talk. *J. Phys. Chem. C* **2015**, *119*, 6670–6677.
- (27) Albers, B. J.; Schwendemann, T. C.; Baykara, M. Z.; Pilet, N.; Liebmann, M.; Altman, E. I.; Schwarz, U. D. Three-Dimensional Imaging of Short-Range Chemical Forces with Picometre Resolution. *Nat. Nanotechnol.* **2009**, *4*, 307–310.
- (28) Albers, B. J.; Schwendemann, T. C.; Baykara, M. Z.; Pilet, N.; Liebmann, M.; Altman, E. I.; Schwarz, U. D. Data Acquisition and Analysis Procedures for High-Resolution Atomic Force Microscopy in Three Dimensions. *Nanotechnology* **2009**, *20*, 264002.
- (29) Baykara, M. Z.; Dagdeviren, O. E.; Schwendemann, T. C.; Möning, H.; Altman, E. I.; Schwarz, U. D. Probing Three-Dimensional Surface Force Fields with Atomic Resolution: Measurement Strategies,

- Limitations, and Artifact Reduction. *Beilstein J. Nanotechnol.* **2012**, *3*, 637–650.
- (30) Baykara, M. Z.; Todorović, M.; Mönig, H.; Schwendemann, T. C.; Ünverdi, O.; Rodrigo, L.; Altman, E. I.; Pérez, R.; Schwarz, U. D. Atom-Specific Forces and Defect Identification on Surface-Oxidized Cu(100) with Combined 3D-AFM and STM Measurements. *Phys. Rev. B: Condens. Matter Mater. Phys.* **2013**, *87*, 155414.
- (31) Mönig, H.; Todorović, M.; Baykara, M. Z.; Schwendemann, T. C.; Rodrigo, L.; Altman, E. I.; Pérez, R.; Schwarz, U. D. Understanding Scanning Tunneling Microscopy Contrast Mechanisms on Metal Oxides: A Case Study. *ACS Nano* **2013**, *7*, 10233–10244.
- (32) Bamidele, J.; Kinoshita, Y.; Turanský, R.; Lee, S. H.; Naitoh, Y.; Li, Y. J.; Sugawara, Y.; Štich, I.; Kantorovich, L. Image Formation and Contrast Inversion in Noncontact Atomic Force Microscopy Imaging of Oxidized Cu(110) Surfaces. *Phys. Rev. B: Condens. Matter Mater. Phys.* **2014**, *90*, 035410.
- (33) Bamidele, J.; Kinoshita, Y.; Turanský, R.; Lee, S. H.; Naitoh, Y.; Li, Y. J.; Sugawara, Y.; Štich, I.; Kantorovich, L. Chemical Tip Fingerprinting in Scanning Probe Microscopy of an Oxidized Cu(110) Surface. *Phys. Rev. B: Condens. Matter Mater. Phys.* **2012**, *86*, 155422.
- (34) Boneschanscher, M. P.; Hämäläinen, S. K.; Liljeroth, P.; Swart, I. Sample Corrugation Affects the Apparent Bond Lengths in Atomic Force Microscopy. *ACS Nano* **2014**, *8*, 3006–3014.
- (35) Otero, R.; Naitoh, Y.; Rosei, F.; Jiang, P.; Thostrup, P.; Gourdon, A.; Lægsgaard, E.; Stensgaard, I.; Joachim, C.; Besenbacher, F. One-Dimensional Assembly and Selective Orientation of Lander Molecules on an O-Cu Template. *Angew. Chem.* **2004**, *116*, 2144–2147.
- (36) El Garah, M.; Lipton-Duffin, J.; MacLeod, J. M.; Gutzler, R.; Palmino, F.; Luzet, V.; Chérioux, F.; Rosei, F. Self-Assembly of a Halogenated Molecule on Oxide-Passivated Cu(110). *Chem. - Asian J.* **2013**, *8*, 1813–1817.
- (37) Sang, H.; Jarvis, S. P.; Zhou, Z.; Sharp, P.; Moriarty, P.; Wang, J.; Wang, Y.; Kantorovich, L. Identifying Tips for Intramolecular NC-AFM Imaging via *In Situ* Fingerprinting. *Sci. Rep.* **2014**, *4*, 6678.
- (38) de Oteyza, D. G.; Gorman, P.; Chen, Y.-C.; Wickenburg, S.; Riss, A.; Mowbray, D. J.; Etkin, G.; Pedramrazi, Z.; Tsai, H.-Z.; Rubio, A.; et al. Direct Imaging of Covalent Bond Structure in Single-Molecule Chemical Reactions. *Science* **2013**, *340*, 1434–1437.
- (39) Neu, M.; Moll, N.; Gross, L.; Meyer, G.; Giessibl, F. J.; Repp, J. Image Correction for Atomic Force Microscopy Images with Functionalized Tips. *Phys. Rev. B: Condens. Matter Mater. Phys.* **2014**, *89*, 205407.
- (40) Hapala, P.; Ondráček, M.; Stetsovych, O.; Švec, M.; Jelínek, P. In *Noncontact Atomic Force Microscopy*; Morita, S., Giessibl, F. J., Meyer, E., Wiesendanger, R., Eds.; NanoScience and Technology; Springer International Publishing, 2015; pp 29–49.
- (41) Ondráček, M.; Pou, P.; Rozsival, V.; González, C.; Jelínek, P.; Pérez, R. Forces and Currents in Carbon Nanostructures: Are We Imaging Atoms? *Phys. Rev. Lett.* **2011**, *106*, 176101.
- (42) Sushko, M. L.; Gal, A. Y.; Watkins, M.; Shluger, A. L. Modelling of Non-Contact Atomic Force Microscopy Imaging of Individual Molecules on Oxide Surfaces. *Nanotechnology* **2006**, *17*, 2062–2072.
- (43) Kling, F.; Bechstein, R.; Rahe, P.; Kühnle, A. In *Noncontact Atomic Force Microscopy*; Morita, S., Giessibl, F. J., Meyer, E., Wiesendanger, R., Eds.; NanoScience and Technology; Springer International Publishing, 2015; pp 147–171.
- (44) Gao, H.-Y.; Díaz Arado, O.; Mönig, H.; Fuchs, H. *Soft Matter Nanotechnology*; Wiley-VCH Verlag GmbH & Co. KGaA, 2015; pp 1–20.
- (45) Ozaki, T.; Kino, H. Numerical Atomic Basis Orbitals from H to Kr. *Phys. Rev. B: Condens. Matter Mater. Phys.* **2004**, *69*, 195113–19.
- (46) Harl, J.; Kresse, G. Density Functional Theory Studies on Stress Stabilization of the Cu(110) Striped Phase. *Surf. Sci.* **2006**, *600*, 4633–4644.
- (47) Blanco, J. M.; Flores, F.; Pérez, R. STM-theory: Image Potential, Chemistry and Surface Relaxation. *Prog. Surf. Sci.* **2006**, *81*, 403–443.
- (48) Mingo, N.; Jurczyszyn, L.; Garcia-Vidal, F. J.; Saiz-Pardo, R.; de Andres, P. L.; Flores, F.; Wu, S. Y.; More, W. Theory of the Scanning Tunneling Microscope: Xe on Ni and Al. *Phys. Rev. B: Condens. Matter Mater. Phys.* **1996**, *54*, 2225–2235.
- (49) Giessibl, F. J. High-Speed Force Sensor for Force Microscopy and Profilometry Utilizing a Quartz Tuning Fork. *Appl. Phys. Lett.* **1998**, *73*, 3956–3958.
- (50) Sader, J. E.; Jarvis, S. P. Accurate Formulas for Interaction Force and Energy in Frequency Modulation Force Spectroscopy. *Appl. Phys. Lett.* **2004**, *84*, 1801–1803.